Photoanodic Properties of Sol−Gel-Derived Fe_2O_3 Thin Films Containing Dispersed Gold and Silver Particles

Akira Watanabe and Hiromitsu Kozuka*

Department of Materials Science and Engineering, Kansai University, 3-3-35, Yamate-cho, Suita 564-8680, Japan

Received: March 20, 2003; In Final Form: July 9, 2003

α-Fe_2O_3 films containing dispersed Au and Ag particles 5−20 nm in size were prepared on nesa silica glass substrates by the sol−gel method, using solutions of a mole ratio $Fe(NO_3)_3 \cdot 9H_2O$: ($HAuCl_4 \cdot 4H_2O$ or $AgNO_3$): $CH_3COCH_2COCH_3$:$CH_3OCH_2CH_2OH$ = 1:0.06:2:20 as the coating solution. The anodic photocurrent−potential characteristics and the action spectra were investigated in a three-electrode cell employing the film electrode as the working electrode. When the film electrode was illuminated with intense white light, the embedded metal particles did not affect the photoanodic properties of the electrode significantly. When the film electrode was illuminated with weak white light or weak monochromatic light, the metal particles, especially Au particles, enhanced the anodic photocurrent; the Au particles embedded in the electrode enhanced the quantum efficiency, IPCE, by about 8 times at a wavelength of 400 nm. Deposition of Au particles just on the surface of the Fe_2O_3 film also increased the photoanodic current, suggesting that the enhanced photocurrent is provided by the Au particles on the electrode surface, which are supposed to catalytically promote the transfer of the hole in the conduction band of Fe_2O_3 to the electrolyte.

Introduction

A number of studies have been carried out on the photoanodic properties of α-Fe_2O_3 in wet-type solar cells since α-Fe_2O_3 has a relatively small band gap of 2.2 eV and photoelectrochemical stability in aqueous solutions.[1−24] α-Fe_2O_3 has, however, small optical absorption coefficient and carrier mobility, both of which are disadvantages for photoanodic properties.[1,2] Improvements of absorption coefficient and carrier mobility would lead to an increase in quantum efficiency and energy conversion efficiency. Increasing the carrier mobility, however, would be difficult because the minority carrier diffusion length is small at 2−4 nm in α-Fe_2O_3[3] due to the hopping mechanism.[25] An increase in carrier concentration has been attempted by doping α-Fe_2O_3 with various metal cations,[4−11] which often introduce energy traps, however, leading to reduced carrier mobility.

Itoh and Bockris reported that the charge separation in the space charge layer can be promoted in α-Fe_2O_3 thin films by making the film thinner than the space charge layer.[1,2] Nanoporous Fe_2O_3 thin films[12] and thin films comprising oriented Fe_2O_3 nanorods[13] showed higher efficiency in charge separation or lower probability in electron−hole recombination than bulk Fe_2O_3 materials.

Doping wide-gap semiconductors such as TiO_2 with dyes[26−28] and with metal cations[26,29,30] is often done in order to expand the photoresponse to the visible regions. One of the authors previously embedded noble metal nanoparticles in TiO_2 thin films by the sol−gel method, expecting that the visible-light-induced excitation of electrons is enhanced by surface plasma resonance.[31−34] Photoanodic current in the visible regions was very slightly increased by Au particles, and that in the ultraviolet regions was increased by Ag particles, the latter of which was thought to result from catalytic promotion of the hole transfer.[31] Noble metal particles such as Au, Ag, Pt, Pd, and Rh are also known to enhance the photocatalytic activity of semiconductor powders and thin films.[35−40] Therefore, enhancement of photocatalytic activity is also expected when noble metal particles are embedded in α-Fe_2O_3 thin films. In the present study, Au and Ag metal particles were embedded in α-Fe_2O_3 thin films by the sol−gel method, and the effects of the particles on the photoanodic properties were studied in a three-electrode cell.

* To whom correspondence should be addressed. E-mail: kozuka@ipcku.kansai-u.ac.jp.

Experimental Section

Preparation of the Film Electrodes. Thin film electrodes with embedded metal particles were prepared by the following procedure. $Fe(NO_3)_3 \cdot 9H_2O$, $HAuCl_4 \cdot 4H_2O$, $AgNO_3$, $CH_3COCH_2COCH_3$, and $CH_3OCH_2CH_2OH$, all purchased from Wako Pure Chemical Industries, Osaka, Japan, were used as the starting materials. Thin film electrodes with embedded metal particles were prepared from solutions AU006 and AG006 in Table 1, i.e., solutions of a mole ratio of $Fe(NO_3)_3 \cdot 9H_2O$:($HAuCl_4 \cdot 4H_2O$ or $AgNO_3$):$CH_3COCH_2COCH_3$:$CH_3OCH_2CH_2OH$ = 1:0.06:2:20. Gel films were deposited on silica glass substrates coated with nesa (Sb-doped SnO_2) by dip-coating with a substrate withdrawal speed of 3 cm min^{-1}. The thickness of the film thus obtained was 0.04 μm, which was measured with a contact probe surface profilometer (SE3400, Kosaka Laboratory, Tokyo, Japan) in a manner described elsewhere.[41] The gel films were fired at 700 °C for 10 min. For some of the film samples, the dip-coating and firing were repeated.

Thin film electrodes with metal particles deposited on the surface were prepared by the following procedure. First, Fe_2O_3 films were deposited on nesa silica glass substrates using solution FE (Table 1), i.e., the solution of a mole ratio of $Fe(NO_3)_3 \cdot 9H_2O$:$CH_3COCH_2COCH_3$:$CH_3OCH_2CH_2OH$ = 1:2:20. Dip-coating was performed with a substrate withdrawal speed of 3 cm min^{-1}, and the gel film was fired at 700 °C for 10 min.

10.1021/jp0303568 CCC: $25.00
Published on Web 10/25/2003

TABLE 1: Composition of the Starting Solutions for Preparing the Film Electrode Samples

	mole ratio				
solution	$Fe(NO_3)_3 \cdot 9H_2O$	$HAuCl_4 \cdot 4H_2O$	$AgNO_3$	$CH_3COCH_2COCH_3$	$CH_3OCH_2CH_2OH$
for embedded type					
AU006	1	0.06		2	20
AG006	1		0.06	2	20
for deposited type					
FE (base layer)	1			2	20
AU-6 (overlayer)		0.06		2	20
AG-6 (overlayer)			0.06	2	20

Then an overlayer was deposited on the Fe_2O_3 film using gold or silver salt solution, solution AU-6 or AG-6 (Table 1), of a mole ratio of ($HAuCl_4 \cdot 4H_2O$ or $AgNO_3$):$CH_3COCH_2COCH_3$:$CH_3OCH_2CH_2OH$ = 0.06:2:20, where dip-coating at 3 cm min^{-1} and firing at 700 °C for 10 min were carried out.

Characterization. Crystalline phase identification and crystallite size measurement were conducted by X-ray diffraction (XRD) measurement using an X-ray diffractometer (RTP-300, Rigaku, Osaka, Japan) with Cu Kα radiation operated at 50 kV and 150 mA. Electron microscopic observation was made using a transmission electron microscope (TEM) (JEM-2000EX/FX, JEOL, Tokyo, Japan). Optical absorption spectra were measured on the film samples using an optical spectrophotometer (UV-2400PC, Shimadzu, Kyoto, Japan). A bare nesa silica glass substrate was used as the reference.

Photoelectrochemical Measurement. Photoanodic properties of the films were evaluated using a potentiostat (Model HZ3000, Hokuto Denko, Osaka, Japan) controlling the potential of the working electrode of a three-electrode cell. The three-electrode cell consisted of the film electrode, a platinized Pt electrode, and SCE as the working, counter, and reference electrodes, respectively, and of a buffer solution of pH 7, an aqueous solution of 0.2 M $Na_2B_2O_4$, 0.14 M H_2SO_4, and 0.3 M Na_2SO_4, as the supporting electrolyte. For measuring the current−potential curves, a 500 W xenon lamp (Model UXL-500D-0, XB-50101AA-A, UI-502Q, Ushio Denki, Tokyo, Japan) was used for illuminating the electrode sample from the front side of the film. In some cases, the intensity of the incident light was reduced to 0.01% using an ND filter. The potential of the working electrode was scanned from 0 V vs SCE toward the positive side at a rate of 20 mV s^{-1}.

Action spectra of the films were measured at a potential of 0.7 V vs SCE, where the xenon lamp light was monochromatized with a monochromator (Model SPG-100, Shimadzu, Kyoto, Japan). For this measurement, first the film was illuminated for 10 s and then the light was put off. The difference in current before and after putting off the light was taken as the photocurrent. The intensity of the monochromatized light was measured with an optical power meter (Model TQ8210, TQ82107, Advantest, Tokyo, Japan), and the quantum efficiency, IPCE, was calculated by the following equation:

$$\mathrm{IPCE} = \frac{n_{\mathrm{curr}\,\lambda}}{n_{\mathrm{ph\,in.}\,\lambda}} = \frac{I_\lambda hc}{W_\lambda \lambda e} \qquad (1)$$

where $n_{\mathrm{curr}\,\lambda}$ is the number of the electrons flowing per second, $n_{\mathrm{ph\,in.}\,\lambda}$ the number of incident photons per second, I_λ the photocurrent, h the Planck constant, c the speed of light, W_λ the intensity of the light, and e the electric charge of an electron.

Space charge capacities were evaluated at 1 kHz using the potentiostat and a frequency response analyzer (Model FRA-5020, NF Electronic Instruments, Kanagawa, Japan), and a Mott−Schottky plot was made using the measured capacities.

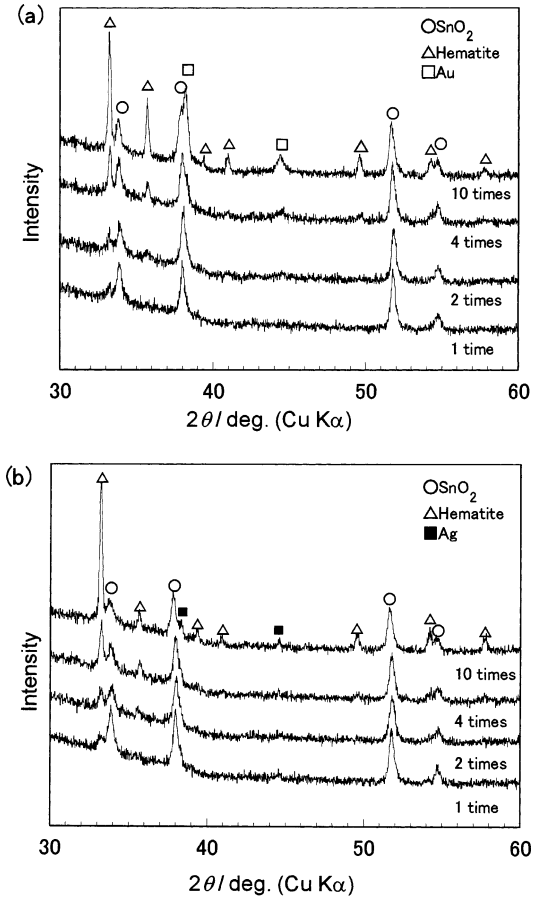

Figure 1. X-ray diffraction patterns of the metal particle-embedded film samples prepared by repeating various times the dip-coating and heat-treatment at 700 °C for 10 min: (a) Au/Fe_2O_3 = 0.03, and (b) Ag/Fe_2O_3 = 0.03. The repeating times are denoted in the figure.

Results

XRD Measurements and TEM Observations. Figure 1 shows the XRD patterns measured on the film electrode samples with embedded metal particles. The samples were prepared from solutions AU006 and AG006 with 1−10 time depositions where dip-coating and firing were cycled. The diffraction peaks of metallic Au and Ag were detected as well as those of hematite. The crystallite size of Au and Ag calculated with Scherrer's equation was 17 and 32 nm, respectively.

Figure 2 shows the TEM pictures of the film electrode samples with embedded metal particles. The samples were prepared from AU006 and AG006 with 1 time deposition. Metal particles of 5−20 nm in size are seen dispersed in the Fe_2O_3 matrix.

Optical Absorption Spectra. Figure 3 shows the optical absorption spectra of the films without metal particles, with embedded metal particles, and with deposited metal particles. For the Au-embedded and -deposited films, optical absorption

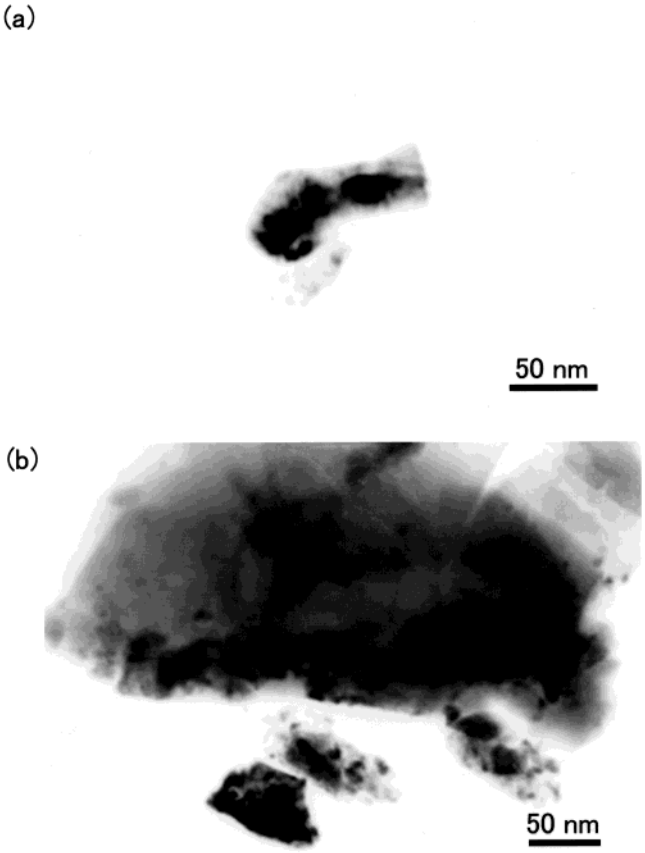

Figure 2. TEM pictures of the metal particle-embedded films prepared from solutions of mole ratios (a) $Au/Fe_2O_3 = 0.03$ and (b) $Ag/Fe_2O_3 = 0.03$.

due to surface plasma resonance was observed at wavelengths around 680 nm. On the other hand, the Ag-embedded or -deposited films showed no evident absorption due to surface plasma resonance. For all the films, the onset of absorption was seen around 590 nm (2.1 eV), a shoulder around 540 nm (2.3 eV), and a peak around 400 nm (3.1 eV). The profile of the spectra obtained for the film without metal particles agree with that of an α-Fe_2O_3 thin film prepared by plasma oxidation of a sputter-deposited iron film.[24] The shoulder around 540 nm and the peak around 400 nm are attributed to the indirect transition and the direct charge transfer from oxygen to iron, respectively.[24]

Band Gap. Band gap energy E_g was obtained for the film without metal particles using the following relation:[42]

$$(Ih\nu)^{n/2} \propto A(h\nu - E_g) \qquad (2)$$

where I is the photoanodic current, $h\nu$ the energy of the incident photon, and A the constant dependent on the potential of the electrode. The photoanodic current I was measured on the action spectra measurement, where the electrode potential was kept constant at 0.7 V vs SCE. $n = 1$ is for direct transition and $n = 1/4$ for indirect transition. Figure 4 shows the $(Ih\nu)^2$ vs $h\nu$ and $(Ih\nu)^{1/2}$ vs $h\nu$ plots, which indicate that the hematite film has a direct band gap of about 2.7 eV and an indirect band gap of about 2.2 eV. These values of the band gap energy agree with those reported by Schumacher on an α-Fe_2O_3 thin film prepared by plasma oxidation of a sputter-deposited iron film.[24]

Photocurrent−Potential Curves Measured under Intense Illumination. Parts a and b of Figure 5 show the photocurrent−potential curves measured on the Au- and Ag-embedded films, respectively. The curve is also shown for the film without metal particles. The measurement was conducted under xenon lamp white light illumination without using the ND filter. Four pieces of the samples were prepared, and the measurement was conducted for each in order to examine the reproducibility of the data. For all the samples the photocurrent onset was found at 0 V vs SCE. The photocurrent decreased and increased very slightly when Au and Ag particles were embedded, respectively.

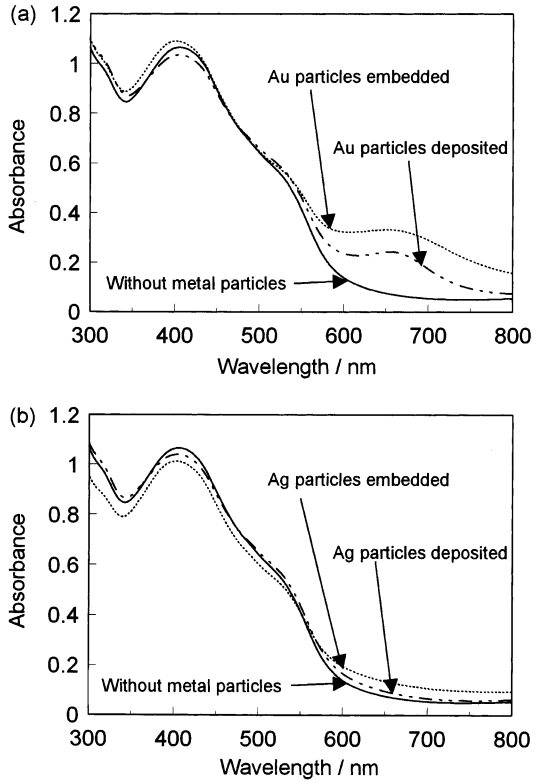

Figure 3. Optical absorption spectra of (a) the Au-embedded and -deposited films and (b) the Ag-embedded and -deposited films, together with the film without metal particles.

Small dark currents were observed at 0.2−0.5 V vs SCE for the Ag-embedded film (Figure 5b), which decreased when the measurement was repeated. The potential agrees with the redox potential of Ag (~0.15 V vs SCE), and Ag-dispersed TiO_2 films also showed small dark currents at similar potentials.[31] Therefore, the dark current observed at 0.2−0.5 V vs SCE is thought to be due to the dissolution of Ag particles.

The photocurrent−potential curves were also measured for the Au- and Ag-deposited films, which are shown in Figure 6. The potential of the photocurrent onset was again 0 V vs SCE. The photocurrent slightly decreased when Au or Ag particles were deposited on the surface of the film. The Au particle deposition resulted in lower photocurrent than the Ag particle deposition.

Photocurrent−Potential Curves under Weak Illumination. Photocurrent−potential curves were also measured under weak white light illumination, where the intensity of the xenon lamp light was reduced to 0.01% with the ND filter. Parts a and b of Figure 7 show the current−potential curves of the film electrode samples with embedded metal particles and those with deposited metal particles, respectively. Either embedding or depositing the metal particles increased the photocurrent, which is recognized as the difference between the currents in light and in dark.

Action Spectra. Figure 8 shows the action spectra of the Au- and Ag-embedded films. Figure 8b is the magnified version of Figure 8a in the visible region. The potential of the film electrodes was kept constant at 0.7 V vs SCE. When Au particles

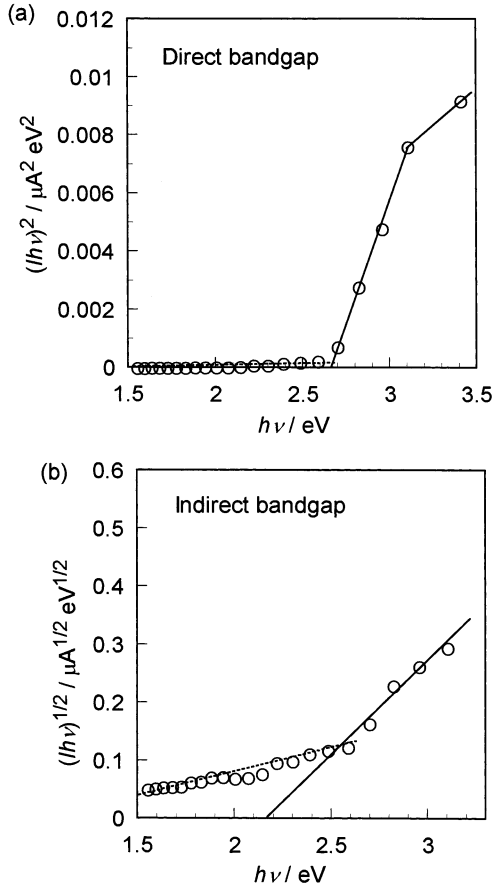

Figure 4. (a) $(Ih\nu)^2$ vs $h\nu$ and (b) $(Ih\nu)^{1/2}$ vs $h\nu$ for the film without metal particles, where I is the photocurrent measured at a potential of 0.7 V vs SCE and $h\nu$ the energy of the incident light.

were embedded, the photoresponse in the ultraviolet region significantly increased by 8 times. A slight increase in photoresponse was also observed at wavelengths around 700 nm by embedding Au particles, where an increase in optical absorption due to surface plasma resonance was observed (Figure 3a). When Ag particles were embedded, on the other hand, the photoresponse in the ultraviolet region increased by 1.5 times, and also a very slight increase in photocurrent was observed at wavelengths around 660 nm.

Mott−Schottky Plot. Figure 9 shows the Mott−Schottky plots of the film without metal particles and the films with embedded metal particles. The flat band potential was found to be −0.3 V vs SCE for all of the samples, and the donor densities were 1.3×10^{19}, 2.1×10^{19}, 1.3×10^{19} cm^{-3} for the film without metal particles, the Au-embedded film, and the Ag-embedded film, respectively.

Transient Photoresponse. Transient photoresponse was studied by chopping the light for the electrode samples in the three-electrode cell. The potential of the working electrode was kept constant at 0.7 V vs SCE in the dark, and 10 min later, the working electrode was illuminated with the xenon lamp white light with or without the ND filter, or with monochromatized light of a wavelength of 400 nm for 10 s. Figure 10 shows the photocurrent transient response of the film without metal particles and those with embedded metal particles. When illuminated with weak white light through the ND filter, all the film electrode samples showed spikes on chopping the light; the spikes increased in the order the Au-embedded film < the film without metal particles < the Ag-embedded film. When illuminated with intense white light, on the other hand, spikes were not observed but gradual photocurrent decay.

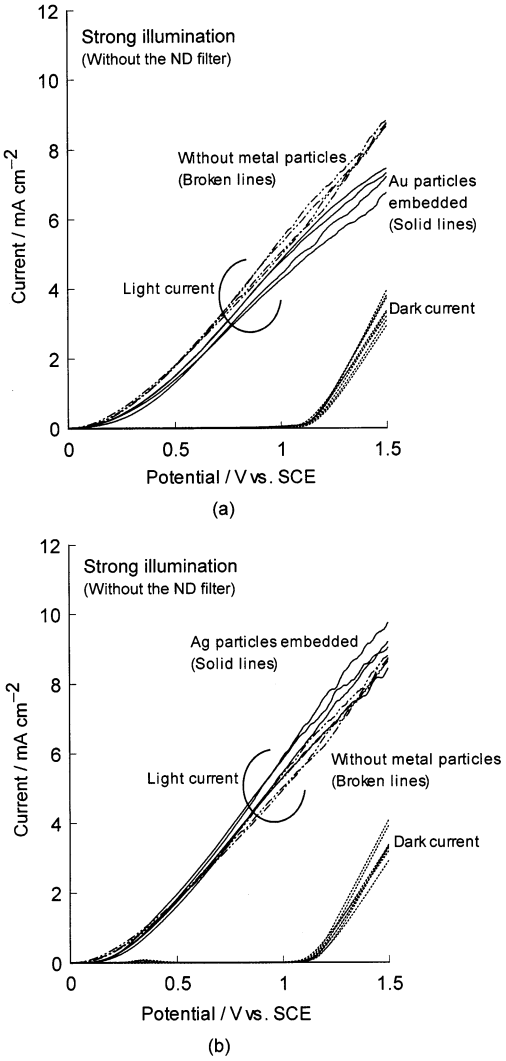

Figure 5. Current−potential curves of (a) the Au-embedded and (b) the Ag-embedded films, together with the film without metal particles, measured under the intense white light without using the ND filter.

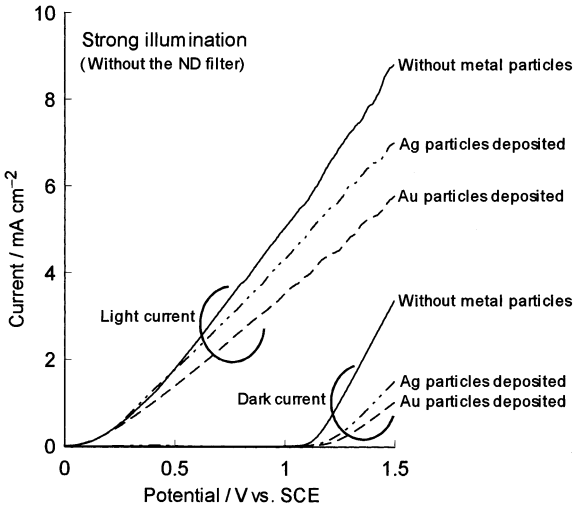

Figure 6. Current−potential curves of the films with metal particles deposited on the electrode surface, together with the film without metal particles, measured under the intense white light without using the ND filter.

Discussion

Band Model Illustration. The band models are illustrated in Figure 11 for the film electrodes with embedded metal

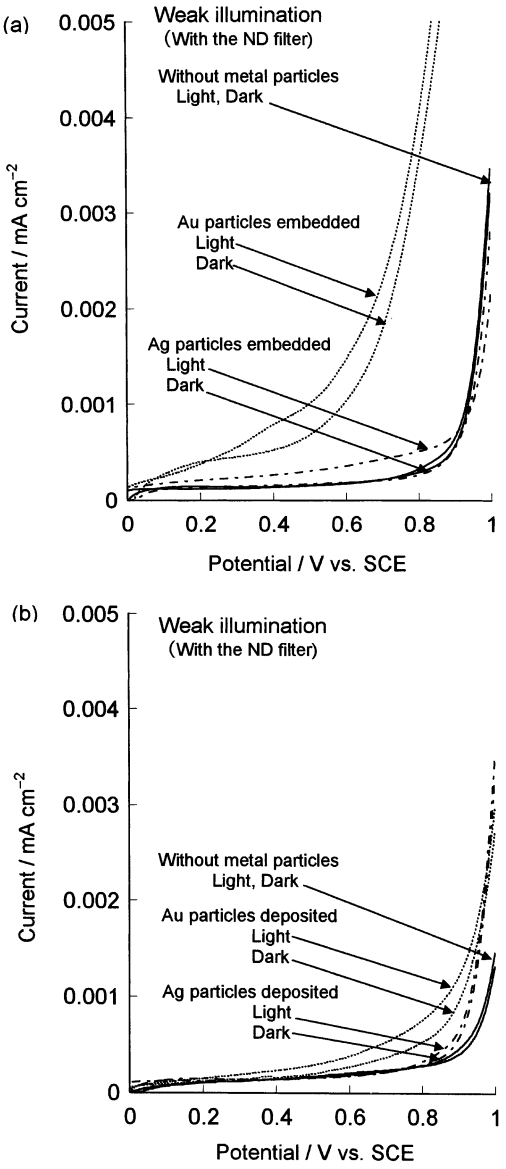

Figure 7. Current−potential curves of the films (a) with embedded metal particles and (b) with metal particles deposited on the surface, together with the film without metal particles, measured under the weak white light through the ND filter.

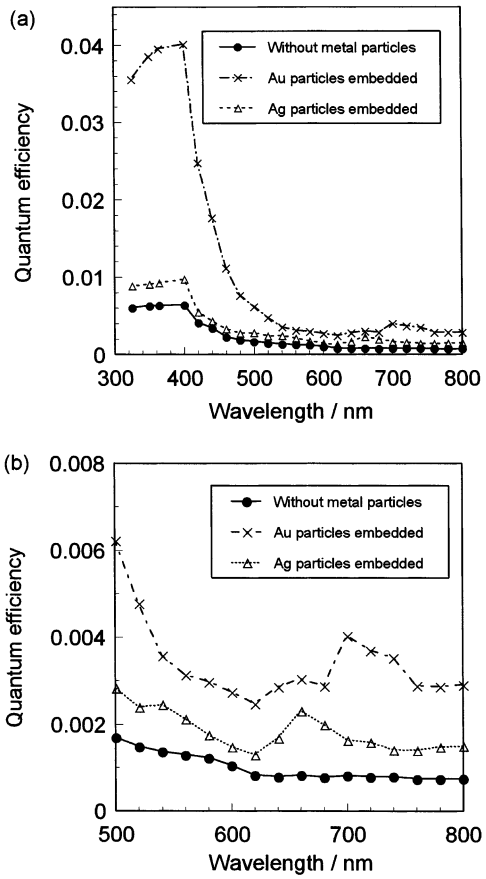

Figure 8. Action spectra of the films with embedded metal particles, together with the film without metal particles, measured at a potential of 0.7 V vs SCE. b is a magnified figure of a.

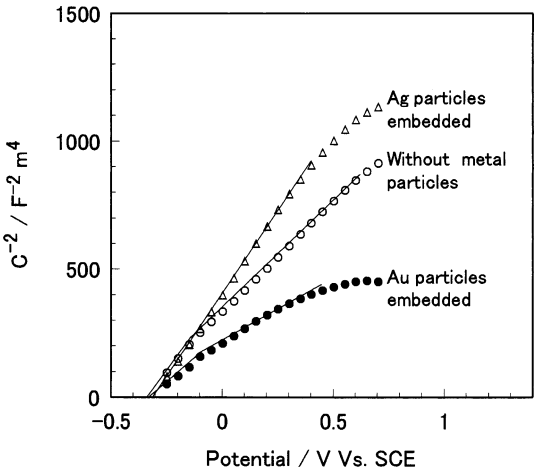

Figure 9. Mott−Schottky plots of the films with embedded metal particles, together with the film without metal particles. The impedance measurement was carried out at a frequency of 1 kHz under dark.

particles at 0.7 V vs SCE, which is the potential applied on the action spectra measurement. First, the band models are considered on the electrodes in dark. The flat band potentials are ca. −0.3 V vs SCE for the Au- and Ag-embedded films as well as for the film without metal particles, which was confirmed in the Mott−Schottky plot (Figure 9). Therefore, the lower edge of the conduction band lies around −0.3 V vs SCE at the film/electrolyte interface. Since the potential of the electrode is assumed to be 0.7 V vs SCE, the lower edge of the conduction band is at around 0.7 V vs SCE in the interior.

The electron affinity of α-Fe_2O_3, χ, is 4.71 eV,[43] and the work functions of Au and Ag, $q\phi_{Au}$ and $q\phi_{Ag}$, are 5.1 and 4.26 eV, respectively.[44] Since the height of the Schottky barrier at the Au/Fe_2O_3 or Ag/Fe_2O_3 interface is determined by the difference in χ and $q\phi_{Au}$ or $q\phi_{Ag}$, the band profiles near the Fe_2O_3/Au or -Ag interface become those like ② and ③ in Figure 11.

Next the band models under illumination are discussed. As discussed by Nakato et al.,[45−50] the photoinduced holes in the valence band diffuses toward the metal particles deposited on the electrode surface, which ends up with depression of the Fermi energy of the surface metals down to the oxygen evolution potential of the corresponding metal electrodes. The oxygen overpotentials of Au and Ag metal electrodes are known to be 0.96 and 0.6 V at an electric current density of 10 mA cm^{-2}.[51] Then, as was studied by Nakato and Tsubomura on a TiO_2 electrode coated with thin metal films,[45] the potentials of Au and Ag particles would positively shift from the O_2/H_2O redox potential (0.57 V vs SCE) by 0.96 and 0.6 V, respectively, as illustrated in Figure 11 when the electrodes are illuminated with intense light.

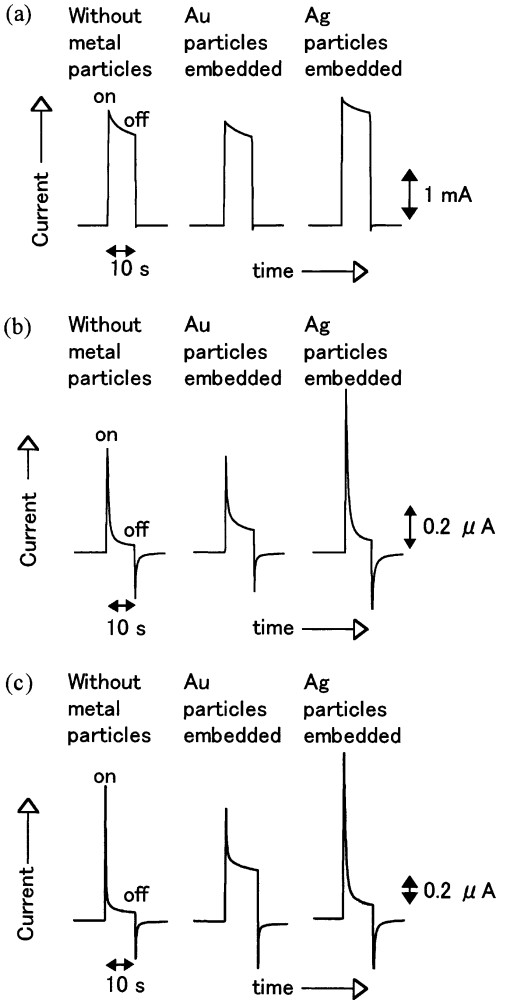

Figure 10. Photocurrent transient response observed under (a) the intense white light without using the ND filter, (b) the weak white light through the ND filter, and (c) the monochromatic light of a wavelength of 400 nm.

Photocurrent Transient Response. As seen in Figure 10, a spike-like transient response was observed in the photocurrent of the film electrode samples when the light was chopped. Similar transient response was also observed previously in α-Fe_2O_3 coating films,[14] amorphous sputtered film,[15] sintered bodies,[16] oxidized films,[16−19] anodic oxidized films,[20] and CVD films.[21] It is thought that such spike-like transient response is caused by the so-called "back-reaction" mechanism described below.[14−21]

In a positively biased n-type semiconductor, the photogenerated holes are trapped in the surface states, reacting with OH^- ions in the supporting electrolyte and forming $OH^•$ radicals adsorbed at the semiconductor surface. The back-reaction is the process where the photogenerated electrons in the conduction band are transferred to and reduce the $OH^•$ radicals and is believed to cause exponential decay of the photocurrent on illumination. The spikes observed on putting off the irradiation are also caused by the transfer of the photogenerated electrons in the conduction band to the $OH^•$ radicals. The whole process of the back-reaction is regarded as the recombination of the photogenerated electrons and holes at the surface states.

As seen in Figure 10, the spikes are significantly large when the incident light is low in intensity. When the light is high in intensity, on the other hand, the photocurrent decay is not large, possibly because the number of photons incident on the electrode is much larger than the electrons trapped in the $OH^•$ radicals.

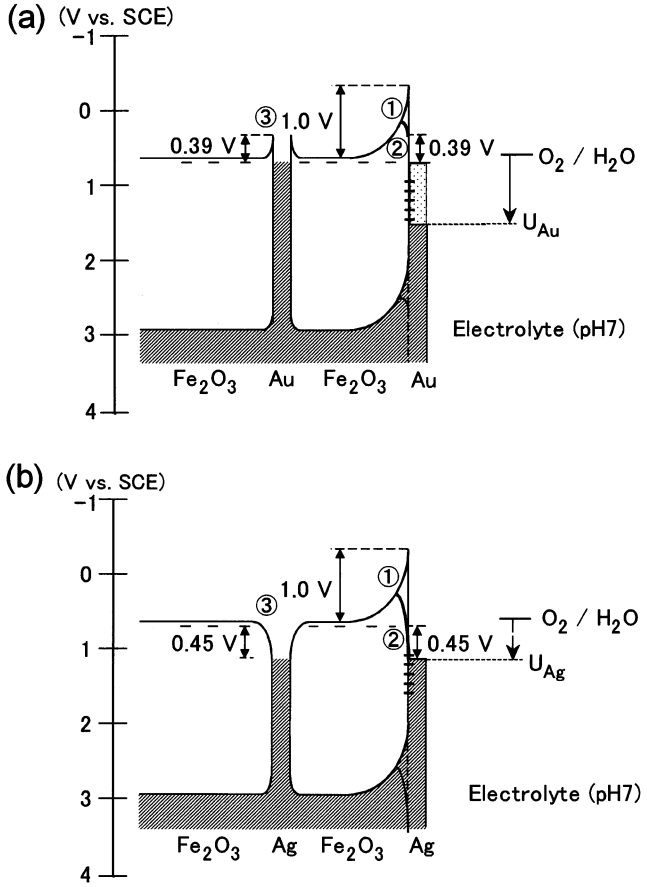

Figure 11. Band model illustrations for (a) the Au- and (b) Ag-embedded films.

As seen in Figure 10 the spikes are relatively large in the Ag-embedded films compared with the Au-embedded film or the film without metal particles. A similar tendency was observed in the films with metal particles deposited on the surface. This may be due to the larger depression of the conduction band at the Ag/Fe_2O_3 interface at the electrode surface denoted by line ② in Figure 11, which promotes the back-reaction, i.e., the electron transfer from the conduction band to the $OH^•$ radicals at the surface.

Effects of the Illumination Intensity and the Metal Particles on the Photoanodic Properties. As seen in Figures 7 and 8, when the illumination intensity was low, the photoresponse was increased by embedding the metal particles, especially Au particles. A Schottky barrier is formed inside the electrode at the metal/Fe_2O_3 interfaces, as shown in Figure 11. The barrier can reduce the electron mobility, not contributing to the enhancement of the photocurrent. When the metal particles were deposited on the electrode surface, the photocurrent also increased, as seen in Figure 7. Therefore, it may be the surface metal particles, not the inner particles, that enhanced the photocurrent. The surface metal particles are thought to promote the hole transfer catalytically from the valence band to the electrolyte, preventing the electron/hole recombination, leading to an increase in photocurrent.

The photoanodic current increased in the order the film with no metal particles < the Ag-embedded film < the Au-embedded film. The band models illustrated in Figure 11 suggest that the conduction band is bent toward lower energies at the metal/Fe_2O_3 interface, more steeply in the Ag-embedded film than in the Au-embedded one, as shown in curves ② in the figure. Such band bending promotes the photoexcited electron transfer from

the conduction band to the electrode surface, causing back-reaction. The steep band bending at the Ag/Fe_2O_3 interface at the electrode surface promotes the back-reaction, which is revealed in the photocurrent transient response (Figure 10). This results in the lower photoanodic current in the Ag-embedded film than in the Au -embedded film. Dissolution of Ag and the resultant reduction in Ag content in the film could also be another reason for the lower photoanodic current in the Ag-embedded film.

When the illumination intensity was high, on the other hand, the effect of the embedded metal particles on the photocurrent was very small (Figure 5), and the deposition of metal particles on the electrode surface rather decreased the photocurrent (Figure 6). As mentioned in the third paragraph of Band Model Illustration, when the electrode is illuminated by highly intense light, the Fermi energy of the surface metal particles can be lowered at maximum in energies down to the oxygen evolution potentials of the corresponding metal electrodes. The depression of the Fermi energy of the surface metal particles can lead to the appearance of the surface states, as illustrated in Figure 11, and the increase in the band bending ② in Figure 11, both of which promote the electron/hole recombination.

It is also noticed that the films with embedded or deposited Ag particles showed a photocurrent slightly higher than those with Au particles (Figures 5 and 6) when illuminated with highly intense light. As was described in the third paragraph of Band Model Illustration, Au particles would have higher potentials (lower energy) than Ag particles on the electrode surface under intense illumination. This would lead to more steep band bending at the metal/semiconductor interface (curve ②, Figure 11) for Au-embedded or -deposited electrodes, promoting the back-reaction, i.e., the transfer of the photogenerated electrons in the conduction band to the $OH^{\bullet}$ radicals.

Photoresponse in the Visible Regions. The Au-embedded film exhibited optical absorption around wavelengths of 680 nm (Figure 3), while the Ag-embedded film did not. The absorption exhibited by the Au-embedded film may result from the surface plasma resonance. However, this would not be the origin of the photoresponse found in the action spectra around 700 nm, because similar photoresponse was also found around 660 nm for the Ag-embedded film, which did not show absorption due to the surface plasma resonance around these wavelengths. Although the origin of the photoresponse in these visible regions is not known, a possible cause is the surface states that are introduced by the metal particles.

Conclusions

α-Fe_2O_3 films containing dispersed Au and Ag particles 5−20 nm in size were prepared on nesa silica glass substrates by the sol−gel method, and the photoanodic properties were studied in a three-electrode cell.

(1) When the film sample was illuminated by intense white light, the embedded metal particles did not affect the photoanodic current significantly.

(2) When the films were illuminated by weak white light or weak monochromatized light, the metal particles, especially Au particles, enhanced the anodic photocurrent; the embedded Au particles enhanced the quantum efficiency by about 8 times at a wavelength of 400 nm.

(3) Deposition of Au particles just on the surface of the Fe_2O_3 film also increased the photoanodic current. This suggests that the enhanced photocurrent in the Au-embedded film is provided by the Au particles on the film surface, which is supposed to promote catalytically the transfer of the hole in the conduction band to the electrolyte.

Acknowledgment. The authors thank Prof. Masahiko Ikeda, Department of Materials Science and Engineering, Kansai University, for his help on TEM observations. H.K. also thanks the Institute of Industrial Technology and the High Technology Research Center of Kansai University for their financial support.

References and Notes

(1) Itoh, K.; Bockris, J. O'M. *J. Appl. Phys.* **1984**, *56*, 874.
(2) Itoh, K.; Bockris, J. O'M. *J. Electrochem. Soc.* **1984**, *131*, 1266.
(3) Kennedy, J. H.; Frese, K. W., Jr. *J. Electrochem. Soc.* **1978**, *125*, 709.
(4) Khan, S. U. M.; Zhou, Z. Y. *J. Electroanal. Chem.* **1993**, *357*, 497.
(5) Kennedy, J. H.; Shinar, R.; Ziegler, J. P. *J. Electrochem. Soc.* **1980**, *127*, 2307.
(6) Shinar, R.; Kennedy, J. H. *Solar Energy Mater.* **1982**, *6*, 323.
(7) Arutyunyan, V. M.; Arakelyan, V. M.; Shakhnazaryan, G. E.; Stepanyan, G. M.; Turner, J. A. *Russ. J. Electrochem.* **1999**, *35*, 854.
(8) Sahami, S.; Kennedy, J. H. *J. Electrochem. Soc.* **1985**, *132*, 1116.
(9) Sastri, M. V. C.; Nagasubramanian, G. *Int. J. Hydrogen Energy* **1982**, *11*, 873.
(10) John, M. R. St.; Tiller, A. J. *J. Electrochem. Soc.* **1985**, *132*, 1859.
(11) Anderman, M.; Kennedy, J. H. In *Semiconductor Electrodes*; Finklea, H. O., Ed.; Elsevier: New York, 1988; Chapter 3.
(12) Bjorksten, U.; Moser, J.; Grätzel, M. *Chem. Mater.* **1994**, *6*, 858.
(13) Beermann, N.; Vayssieres, L.; Lindquist, S.; Hagfeldt, A. *J. Electrochem. Soc.* **2000**, *147*, 2456.
(14) Qian, X.; Zhang, X.; Al, X.; Han, Y.; Liu, F.; Cai, S.; Bai, Y.; Li, T.; Tang, X.; Yao, J. *Mol. Cryst. Liq. Cryst.* **1999**, *337*, 437.
(15) Benko, F. A.; Longo, J.; Koffyberg, F. P. *J. Electrochem. Soc.* **1985**, *132*, 609.
(16) Curran, J. S.; Gissler, W. *J. Electrochem. Soc.* **1979**, *126*, 56.
(17) Iwanski, P.; Curran, J. S.; Gissler, W. *J. Electrochem. Soc.* **1981**, *128*, 2128.
(18) Ray Yeh, L.; Hackerman, N. *J. Electrochem. Soc.* **1977**, *124*, 833.
(19) Wilhelm, S. M.; Yun, K. S.; Ballenger, L. W.; Hackerman, N. *J. Electrochem. Soc.* **1979**, *126*, 419.
(20) Abrantes, L. M.; Peter, L. M. *J. Electroanal. Chem.* **1983**, *150*, 593.
(21) Hardee, K. L.; Bard, A. J. *J. Electrochem. Soc.* **1977**, *124*, 215.
(22) Khan, S. U. M.; Akikusa, J. *J. Phys. Chem. B* **1999**, *103*, 7184.
(23) Sammells, A. F.; Ang, P. G. P. *J. Electrochem. Soc.* **1979**, *126*, 1831.
(24) Schumacher, L. C.; Mamiche-Afara, S.; Weber, M. F.; Dignam, M. J. *J. Electrochem. Soc.* **1985**, *132*, 2945.
(25) Gleitzer, C.; Nowrotny, J.; Rekas, M. *Appl. Phys.* **1991**, *53*, 310.
(26) Finklea, H. O. In *Semiconductor Electrodes*; Finklea, H. O., Ed.; Elsevier: New York, 1988; Chapter 2.
(27) Zaban, A.; Ferrere, S.; Gregg, B. A. *J. Phys. Chem. B* **1998**, *102*, 452.
(28) Haque, S. A.; Tachibana, Y.; Klug, D. R.; Durrant, J. R. *J. Phys. Chem. B* **1998**, *102*, 1745.
(29) Monnier, A.; Augustynski, J. *J. Electrochem. Soc.* **1980**, *127*, 1576.
(30) Matsumoto, Y.; Shimizu, T.; Toyoda, A.; Sato, E. *J. Phys. Chem.* **1982**, *86*, 3581.
(31) Zhao, G.; Kozuka, H.; Yoko, T. *Thin Solid Films* **1996**, *277*, 147.
(32) Zhao, G.; Kozuka, H.; Yoko, T. *J. Ceram. Soc. Jpn.* **1996**, *104*, 164.
(33) Zhao, G.; Kozuka, H.; Yoko, T. *Solar Energy Mater. Solar Cells* **1997**, *46*, 219.
(34) Kozuka, H. *SPIE* **1997**, *3136*, 304.
(35) Wold, A. *Chem. Mater.* **1993**, *5*, 280.
(36) Andreeva, D.; Idakiev, V.; Tabakova, T.; Christov, P.; Giovanoli, R. *Appl. Catal. A* **1998**, *169*, 9.
(37) Andreeva, D.; Idakiev, V.; Tabakova, T.; Andreev, A.; Giovanoli, R. *Appl. Catal. A* **1996**, *134*, 275.
(38) Gao, Y.-M.; Lee, W.; Trehan, R.; Kershaw, R.; Dwight, K.; Wold, A. *Mater. Res. Bull.* **1991**, *26*, 1247.
(39) Herramann, J.-M.; Disdier, J.; Pichat, P.; Fernandez, A.; Gonzalez-Elipe, A.; Munuera, G.; Leclercq, C. *J. Catal.* **1991**, *132*, 490.
(40) Lee, W.; Shen, H.-S.; Dwight, K.; Wold, A. *J. Solid State Chem.* **1993**, *106*, 288.
(41) Kozuka, H.; Kajimura, M. *J. Am. Ceram. Soc.* **2000**, *83*, 1056.
(42) Butler, M. A.; Ginley, D. S. *J. Appl. Phys.* **1977**, *48*, 3070.
(43) Liou, F.-T.; Yang, C. Y. *J. Electrochem. Soc.* **1982**, *129*, 342.
(44) *Kagaku-Binran, 4th ed.; Kiso-hen II*; The Chemical Society of Japan, Eds.; Maruzen: Tokyo, Japan, 1993; p 489 [in Japanese].
(45) Nakato, Y.; Tsubomura, H. *Isr. J. Chem.* **1982**, *22*, 180.

(46) Nakato, Y.; Shioji, M.; Tsubomura, H. *Chem. Phys. Lett.* **1982**, *90*, 453.
(47) Nakato, Y.; Tsubomura, H. *J. Photochem.* **1985**, *29*, 257.
(48) Nakato, Y.; Abe, K.; Tsubomura, H. *Ber. Bunsen-Ges. Phys. Chem.* **1976**, *80*, 1002.
(49) Nakato, Y.; Ueda, K.; Yano, H.; Tsubomura, H. *J. Phys. Chem.* **1988**, *92*, 2316.
(50) Nakato, Y.; Tsubomura, H. *Electrochem. Acta* **1992**, *37*, 897.
(51) *Denki-Kagaku-Binran*; The Electrochemical Society of Japan, Eds.; Maruzen: Tokyo, Japan, 1964; p 729 [in Japanese].